Pion density in nuclei and deep-inelastic lepton scattering

E. L. Berger,* F. Coester,† and R. B. Wiringa†
Argonne National Laboratory, Argonne, Illinois 60439
(Received 15 July 1983)

Recent data indicate that quark densities in a high-A nucleus differ significantly from those measured in the free-nucleon case. We examine whether this effect can be explained in terms of deep-inelastic scattering from mesons responsible for nuclear binding. Although features of the data are reproduced qualitatively, we are unable to approach a quantitative description of the magnitude of the experimental effect at small x unless we postulate an enhanced pion density of about 0.4 extra pions per nucleon (roughly three times that provided by conventional nuclear models), and/or make assumptions about the small-x behavior of the meson structure function which are inconsistent with available data. These conclusions are insensitive to the manner in which we impose momentum conservation. The slope of the ratio of structure functions vs x is reproduced easily in the range $0.05 < x < 0.5$. We speculate that a quantitative fit to the data requires an "intrinsic" enhancement of the nucleon structure function due to the nuclear medium as well as scattering from the mesons associated with binding.

I. INTRODUCTION

The inelastic structure function $F_2(x,Q^2)$ for deep-inelastic muon scattering from an iron nucleus is observed to differ markedly from the structure function for deuterium.[1] Here Q^2 is the usual square of the invariant four-momentum transfer and $x = Q^2/2M\nu$, where ν is the laboratory energy transfer. There are potentially important implications of this result for both theories of nuclear structure and phenomenological models of high-energy inclusive scattering. When interpreted in terms of the quark-parton model, the deep-inelastic data imply that the nucleon's sea quark and antiquark densities are enhanced in a nucleus, whereas the momentum carried by valence quarks is degraded.[2] This result was not generally expected.[3] It raises the possibility that nuclear medium significantly alters the behavior of the pointlike constituents of the nucleons.[4]

An alternative explanation is suggested by the conventional picture of nuclei as systems of nucleons and mesons. Deep-inelastic lepton scattering may occur either from constituents of the nucleons or from constituents of the mesons.[5] The mesons are associated with the exchange mechanisms responsible for nuclear binding. In this paper we examine whether a quantitative interpretation of the data can be obtained in terms of this conventional meson-nucleon picture.

In Fig. 1, we provide a rough sketch of the physical process through which the virtual photon of deep-inelastic scattering interacts with an exchanged meson within a nucleus. We assume throughout that we are dealing with an "isoscalar" nucleus, viz., a nucleus with equal numbers of neutrons and protons. The solid horizontal lines in Fig. 1 represent either nucleons or nucleon isobars [e.g., $\Delta(1238)$]. There are three main ingredients in the approach we study. First, we assume that nuclei are bound systems of nucleons and mesons. Second, we assume that the deep-inelastic structure functions of these nucleons and mesons are unaffected by the nuclear medium; in our calculations we employ structure functions measured on isolated nucleons and pions. Third, we retain the usual assumption that nucleons contribute incoherently to the structure function of the nucleus, and we add the same incoherence assumption for the mesons. It follows that we can write the nuclear structure function as a sum of convolutions of isolated-hadron structure functions with meson and nucleon momentum distributions derived from specific nuclear models. Thus, our final prediction for the nuclear structure function per nucleon is cast in the form

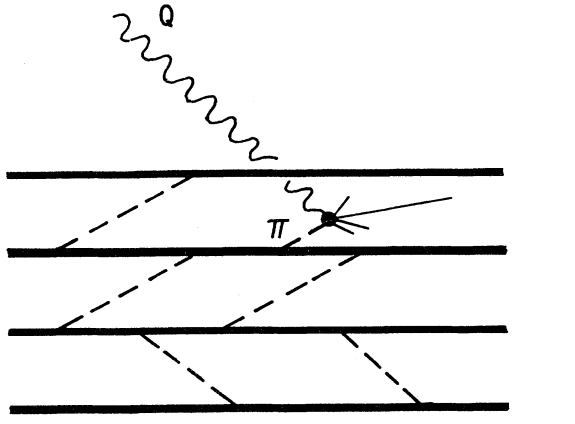

FIG. 1. Virtual photon carrying four-vector momentum Q interacts with one of the meson exchanges (dashed lines) in a nucleus. The thick horizontal lines represent nucleons or nucleon isobars in the nucleus. Thin solid lines suggest the deep-inelastic breakup of the meson.

$$F_2^A(x,Q^2)=\int_x f_\pi(y)F_2^\pi\left[\frac{x}{y},Q^2\right]dy + \int_x f_N(z)F_2^N\left[\frac{x}{z},Q^2\right]dz \ . \quad (1.1)$$

In Eq. (1.1), $F_2^N(x,Q^2)$ and $F_2^\pi(x,Q^2)$ are structure functions measured on unbound nucleons and mesons, respectively, at some specified value of Q^2. Our goal, addressed in Secs. III and IV, is to derive expressions for the magnitudes and momentum dependences of $f_\pi(y)$ and $f_N(z)$ which represent the densities of mesons and nucleons carrying fractional longitudinal momenta y and z. Precise definitions for y and z are provided below. The integral $\langle n_\pi\rangle=\int yf_\pi(y)dy$ is the mean number of *excess* mesons *per nucleon* associated with nuclear binding, and $\langle y\rangle\equiv\int yf_\pi(y)dy$ is the fraction per nucleon of the momentum of the nucleus carried by the excess mesons.

In Sec. II we present the free-nucleon and -meson structure functions which we use in our numerical work. We also discuss salient qualitative features of the data, including the magnitude and slope of the ratio $R(x)$ of the nuclear structure function to that for deuterium. These remarks suffice to show that a quantitative description of $R(x)$ at $x\simeq 0.05$ requires values of $\langle n_\pi\rangle$ in excess of $\langle n_\pi\rangle\simeq 0.2$. We conclude Sec. II with the presentation of a "toy model" which illustrates the roles of the two terms on the right-hand side of Eq. (1.1).

In Sec. III, we demonstrate formally that the structure function of a compound system, whose constituents contribute incoherently, may be expressed directly in terms of the structure functions of the constituents and the wave function of the compound system. For large Q^2, this analysis yields an equation of the form of Eq. (1.1) in which $f_\pi(y)$, $F_2^\pi(x)$ and $f_N(z)$, $F_2^N(x)$ are momentum densities and structure functions of the constituent pions and (bare) nucleons. To apply this result in the manner outlined above, we must include the pion clouds (if any) of individual nucleons as part of the nucleon structure and identify $f_\pi(y)$ with the *excess* density of pions.

To derive this excess density $f_\pi(y)$ we begin in Sec. IV by defining a momentum-dependent meson-density operator and then we evaluate its expectation value using nuclear many-body wave functions. We expect the bulk of the relevant meson effects in deep-inelastic scattering to be associated with long-range one-pion and intermediate-range attractive two-pion exchange. A substantial fraction of the two-pion attraction can be incorporated by including Δ isobar states and the one-pion exchanges associated with $N\Delta\pi$ and $\Delta\Delta\pi$ vertices. We consider therefore a nuclear Hamiltonian which includes $NN\pi$, $N\Delta\pi$, and $\Delta\Delta\pi$ vertices. From this, we derive an effective meson-exchange potential. The *excess* pion density is then obtained by calculating the linear response of the potential energy to a change in the pion's energy. The approximations used in deriving the potential are also used consistently in deriving the associated pion densities. In Sec. IV, we also discuss models for $f_N(z)$, the nucleon momentum distribution in a nucleus.

Our conclusions, summarized in Sec. V, are that some qualitative features of the data are reproduced. However, we find that the magnitude of the experimental effect at very small x ($\lesssim 0.1$) cannot be obtained unless we postulate an enhanced pion density of about $\langle n_\pi\rangle=0.4$ extra pions per nucleon. This value is roughly three times that which is calculated from the conventional nuclear models which we study and is considered excessive. Furthermore, even with this large value of $\langle n_\pi\rangle$, we are unable to fit the full x dependence of the ratio of structure functions. This discrepancy becomes serious for modest values of x ($x\cong 0.2$ to 0.3). These difficulties are insensitive to changes in both $\langle n_\pi\rangle$ and the average value $\langle y\rangle$, and to the manner in which we enforce momentum balance between the nucleon and meson constituents of the nucleus. Consequently, we believe that the data contradict our (second) assumption that the deep-inelastic structure functions of nucleons are unaffected by the nuclear medium. We speculate that there are two perhaps equally important contributions to the enhancement of $F_2^A(x)$ at relatively small x. One is related to scattering from the mesons in the nucleus. The second is an "intrinsic" distortion of the nucleon structure function associated with the nuclear medium.

II. PHENOMENOLOGY

The data[1] of interest are shown in Fig. 2. They are presented as a ratio $R(x)$ of the structure functions, per nucleon, observed in deep-inelastic scattering from iron and deuterium targets. Since Fe and D each contain approximately equal numbers of neutrons and protons, and, thus, equal numbers of up and down quarks, the effect shown in Fig. 2 is not associated with a difference in the x dependences of up- and down-quark densities $u(x)$ and $d(x)$. Traditional interpretations of the quark-parton model led to the expectation that $R(x)$ would be very nearly unity and show no significant dependence on x for $x\gtrsim 0.05$.[3,6,7] It is unclear, *a priori,* whether the effect shown in Fig. 2 is due principally to the numerator (Fe) or the denominator (D). Since our computations in Sec. IV indicate that the number of excess mesons per nucleon is negligible in D, our approach to the physics presupposes that the effect in $R(x)$ is associated with the heavy Fe nucleus. However, since we are unable to provide a satisfactory quantitative explanation of the data, we can only *postulate* that the numerator is the principle agent.

We shall assume here that a nucleus consists of on-mass-shell nucleons and pions, the pions being associated with the meson exchange forces responsible for nuclear binding. We implicitly ignore both the pionic self-energy and the pionic density associated with the mesonic cloud of isolated nucleons, and thus we deal only with *excess* mesons associated with binding. We define a light-front momentum fraction per nucleon,

$$y=\frac{A(E+p_L)_\pi}{(E+p_L)_A} \quad (2.1)$$

for pions, and a similar quantity for nucleons,

$$z=\frac{A(E+p_L)_N}{(E+p_L)_A} \ . \quad (2.2)$$

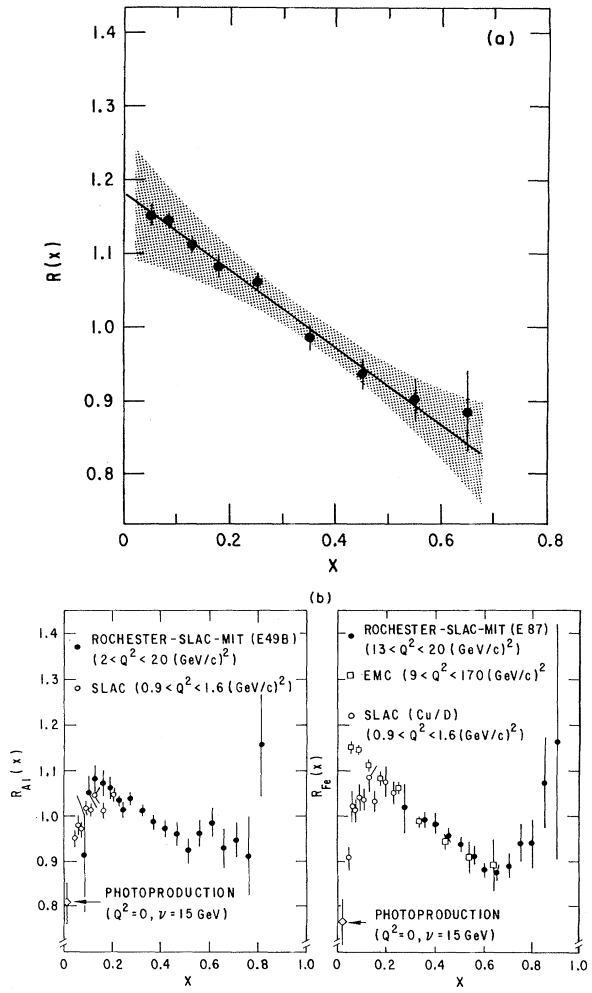

FIG. 2. (a) Data from the CERN European Muon Collaboration for $R(x)=F_2(\mathrm{Fe})/F_2(\mathrm{D})$, from Ref. 1. The shaded band indicates the range of probable systematic uncertainties. (b) Compilation of data on $R(x)$ for Al and for Fe, taken from Bodek *et al.* (Ref. 1).

Here E and p_L are the energy and longitudinal momentum components of four-vector momenta; A is the number of nucleons. The subscript A is used to denote the entire nucleus. Functions $f_N(z)$ and $f_\pi(y)$ are defined to specify the number densities, per nucleon, of nucleons and excess mesons in the nucleus with momentum fractions z and y, respectively. The mean number of excess pions per nucleon is

$$\langle n_\pi \rangle = \int f_\pi(y)dy \ . \tag{2.3}$$

The mean number of nucleons, per nucleon, is obviously unity. Thus, the function $f_N(z)$ satisfies the normalization integral

$$\int f_N(z)dz = 1 \ . \tag{2.4}$$

Conservation of momentum requires that

$$\int y f_\pi(y)dy + \int z f_N(z)dz = 1 \ . \tag{2.5}$$

The variables y and z range over the interval 0 to A, but, in practice, $f_\pi(y)$ has its main support for $y<1$, and $f_N(z)$ has its main support in the neighborhood of $z=1$.

In terms of the picture presented here, the structure function $F_2^A(x)$ extracted from data obtained on a nuclear target receives contributions from two sources. The deep-inelastic virtual photon interacts either with a pion or with a nucleon in the nucleus. Equation (1.1) is derived in Sec. III for large Q^2 under the assumptions that the nucleus is a bound system of A nucleons and an indefinite number of pions, and that the nucleons and pions contribute incoherently to the structure function of the nucleus. We note that the integral $\int F_2^A(x)dx$ is not necessarily left invariant. Employing Eq. (2.5) one may show that

$$\int F_2^A(x)dx = \int F_2^N(x)dx$$

only if

$$\int F_2^\pi(x)dx = \int F_2^N(x)dx$$

or if

$$\langle y \rangle = \int y f_\pi(y)dy = 0 \ .$$

The predicted ratio $R(x)=F_2^A(x)/F_2^N(x)$ takes on a particularly simple form at exactly $x=0$. From Eqs. (1.1), (2.3), and (2.4), we deduce

$$R(0) \equiv \frac{F_2^A(0)}{F_2^N(0)} = 1 + \langle n_\pi \rangle \frac{F_2^\pi(0)}{F_2^N(0)} \ . \tag{2.6}$$

Correspondingly, if a straight-line fit to the data in Fig. 2 is extended naively to $x=0$, we would deduce an immediate bound on $\langle n_\pi \rangle$, as long as $F_2^\pi(0)/F_2^N(0)$ is assumed to be known.

There are difficulties associated with a straightforward application of Eq. (2.6). In the quark-parton model, $F_2(x)$ receives contributions from both valence and ocean components of the quark and antiquark densities. The valence components are usually parametrized so that their contribution to $F_2(x)$ vanishes at $x=0$. The ratio $F_2^\pi(x)/F_2^N(x)$ at precisely $x=0$ is therefore determined entirely by the ocean components whose values at $x=0$ are not known to great precision. However, for $x \gtrsim 0.05$, the valence components are comparable to the ocean components, and the value of $F_2^\pi(x)/F_2^N(x)$ *extrapolated* to $x=0$ from, say, the region $0.05 \leq x \leq 0.3$ over which the experimental $R(x)$ is roughly linear, is controlled by both the valence and the ocean components of $F_2^\pi(x)$ and $F_2^N(x)$. Later in this section we present explicit parametrizations for $F_2^N(x)$ and $F_2^\pi(x)$ from which we deduce that the ratio $F_2^N(x)/F_2^\pi(x)$ extrapolated to $x=0$ lies in the range of 1.3 to 2.0. Consequently, $\langle n_\pi \rangle$ must be greater than $R(0)-1$ by approximately this factor.

Second, in addition to effects associated with the ocean at very small x, another reason for avoiding the very-small-x region in the data is the possibility that important shadowing effects,[1,6,7] not included in our description, may control the precise $x=0$ behavior of $R(x)$. A suggestive method for avoiding these two difficulties is to

rewrite Eq. (2.6) as

$$\langle n_\pi \rangle \overset{\text{extrap}}{\underset{x\to 0}{=}} \left\{ \frac{F_2^N(x)}{F_2^\pi(x)} [R(x)-1] \right\} , \tag{2.7}$$

where the extrapolation procedure in Eq. (2.7) is understood to imply a fit to the data for $x \gtrsim 0.05$, whose results are then extended to $x=0$ in a straightforward way. This method would work well in our case if our theoretical $R(x)$ behaved very smoothly over the range $x=0$ to, say, $x=0.2$. However, as discussed in Sec. II C, the derivative $\partial R/\partial x$ of our theoretical $R(x)$ changes rather rapidly with x in the region $x \lesssim 0.05$. Our Eq. (2.6), is, of course, still correct, but, owing to the rapid variation of $\partial R/\partial x$, the appropriate value of $\langle n_\pi \rangle$ cannot be deduced from the extrapolation to $x=0$ of a simple linear fit to the data. Instead, one obtains a *lower* bound on $\langle n_\pi \rangle$ from the method indicated in Eq. (2.7).

The fit shown in Fig. 2 to the CERN European Muon Collaboration (EMC) data yields an extrapolated central value $R_{\text{Fe}}(0)=1.18$. There is large spread associated with systematic uncertainties such that

$$R_{\text{Fe}}^{\text{EMC}}(0)=1.18\pm 0.09 . \tag{2.8}$$

From fits to their data in the range $0.2<x<0.6$ (with $4 \lesssim Q^2 \lesssim 20$ GeV^2), the Rochester-SLAC-MIT collaboration quotes intercepts at $x=0$ of

$$R_{\text{Al}}(0)=1.10\pm 0.02 , \tag{2.9}$$

$$R_{\text{Fe}}(0)=1.15\pm 0.04 . \tag{2.10}$$

Probable systematic errors associated with overall normalization uncertainties are not included in Eqs. (2.9) and (2.10). Taken at face value, Eqs. (2.7), (2.9), and (2.10) imply that

$$\frac{\langle n_\pi(\text{Al}) \rangle}{\langle n_\pi(\text{Fe}) \rangle} \simeq \frac{2}{3} , \tag{2.11}$$

but the probable errors do not exclude unity.

A. Digression: Pion and nucleon structure functions

In this subsection we specify the pion and nucleon structure functions $F_2^\pi(x,Q^2)$ and $F_2^N(x,Q^2)$ used throughout our analysis. As was suggested in the last paragraph, quantitative conclusions regarding $\langle n_\pi \rangle$ depend in some detail on what is known and not known about $F_2^\pi(x)$ and $F_2^N(x)$.

In the quark-parton model, $F_2(x,Q^2)$ may be expressed as a sum over contributions from the different quark and antiquark flavors:

$$F_2(x,Q^2)=x \sum_f e_f{}^2 [q_f(x,Q^2)+\bar{q}_f(x,Q^2)] . \tag{2.12}$$

Here e_f denotes the fractional charge of the quark of flavor, f and $q_f(\bar{q}_f)$ are the quark (antiquark) probability distributions. For the nucleon's quark and antiquark densities we use the explicit parametrizations derived by the CERN-Dortmund-Heidelberg-Saclay (CDHS) collaboration[8] from fits to deep-inelastic νH_2 and $\bar{\nu} H_2$ data.

Our isoscalar nucleus contains equal numbers of protons and neutrons. Thus, the up, down, and strange quark and antiquark densities in each effectively isoscalar nucleon are expressed in terms of valence $V_N(x)$ and ocean $S_N(x)$ components as

$$u_N(x)=d_N(x)=V_N(x)+S_N(x) , \tag{2.13}$$

$$\bar{u}_N(x)=\bar{d}_N(x)=s_N(x)=\bar{s}_N(x)=S_N(x) . \tag{2.14}$$

The Q^2 dependence has been suppressed in Eqs. (2.13) and (2.14); Eq. (2.14) expresses our assumption of SU(3) symmetry for the ocean.[9] We ignore the charm ocean. For $V_N(x)$, we adopt

$$V_N(x)=\tfrac{3}{8}[u_p(x)+2d_p(x)] , \tag{2.15}$$

where $u_p(x)$ and $d_p(x)$ are the up and down valence components of the *proton* structure function, as determined by the CDHS group. Because the total number of valence quarks in a nucleon is three, we have

$$\int V_N(x)dx = \tfrac{3}{2} . \tag{2.16}$$

For $S_N(x)$ we use the expression for $\bar{u}_N(x)$ determined in the CDHS analysis. The ocean and valence components together carry 45% of the nucleon's momentum at $Q^2=25$ GeV^2.

In terms of Eqs. (2.13) and (2.14), we obtain

$$F_2^N(x,Q^2)=x[\tfrac{5}{9}V_N(x,Q^2)+\tfrac{4}{3}S_N(x,Q^2)] . \tag{2.17}$$

Since the pion quark densities, discussed below, are determined only at $Q^2 \simeq 25$ GeV^2, we choose for reasons of consistency to evaluate the CDHS nucleon quark densities also at $|Q^2|=25$ GeV^2. The EMC data in Fig. 2 are specified at an *average* $Q^2 \simeq 50$ GeV^2, with $\langle Q^2 \rangle$ increasing with x. Since no appreciable dependence on Q^2 is observed in the data, we believe our choice of $Q^2=25$ GeV^2 for our calculations does not bias our conclusions. To discuss Q^2 dependence at fixed x, we would need a set of pion structure functions whose evolution with Q^2 is known to roughly the same degree of precision as that of the CDHS nucleon structure functions.

There are no measurements of deep-inelastic lepton scattering from pion targets, except possibly for the data discussed in this paper. However, if the Drell-Yan model is assumed to apply, structure functions may be extracted from data on massive lepton pair production $\pi N \to \gamma^* X$. A detailed analysis of this type was performed by the CERN NA3 collaboration,[10] resulting in a determination of the effective valence and ocean components of the pion quark and antiquark densities at a mean $Q^2=25$ GeV^2. We shall use these NA3 functions in our analysis.[11]

Because we are describing isoscalar nuclei, our pions are also "isoscalar" mesons containing equal numbers of up, down, anti-up, and anti-down quarks. Decomposing $q_f^{(\pi)}(x)$ into valence $V_\pi(x)$ and ocean $S_\pi(x)$ components, we write

$$u_\pi(x)=\bar{u}_\pi(x)=d_\pi(x)=\bar{d}_\pi(x) = \tfrac{1}{2}V_\pi(x)+S_\pi(x) , \tag{2.18}$$

$$s_\pi(x)=\bar{s}_\pi(x)=S_\pi(x) . \tag{2.19}$$

Since the number of valence quarks plus valence antiquarks in a pion is two, our normalization is

$$\int_0^1 V_\pi(x)dx = 1 \ . \tag{2.20}$$

We assume the ocean in the pion to be SU(3) symmetric.[9] We obtain

$$F_2^{(\pi)}(x) = x[\tfrac{5}{9}V_\pi(x) + \tfrac{4}{3}S_\pi(x)] \ , \tag{2.21}$$

identical in form to Eq. (2.17).

The specific NA3 parametrizations[10,11] of $V_\pi(x)$ and $S_\pi(x)$ which we use are

$$xV_\pi(x) = \frac{\Gamma(\alpha+\beta+1)}{\Gamma(\alpha)\Gamma(\beta+1)} x^\alpha (1-x)^\beta \ , \tag{2.22}$$

with $\alpha = 0.41$ and $\beta = 0.95$, and

$$xS_\pi(x) = \frac{A_s}{6}(p+1)(1-x)^p \ , \tag{2.23}$$

with $p = 8.4$, and $A_s = 0.183$. Together the valence and sea quarks carry 53% of the pion's momentum; the ocean alone carries 18.3%.

The functions $F_2^\pi(x)$ and $F_2^N(x)$ are shown in Fig. 3. The ocean contributes more than half of $F_2^N(x)$ for $x \lesssim 0.06$ after which its importance dies away very rapidly as x grows. For $F_2^\pi(x)$, the ocean dominates until $x \simeq 0.13$ after which the valence component takes over rapidly with increasing x. The larger magnitude of $V_N(x)$ relative to $V_\pi(x)$ at modest values of x ($x \lesssim 0.3$) is understood easily in terms of Eqs. (2.16) and (2.20), plus the application of constituent counting rules[12] which suggest that $V_N(x) \sim (1-x)^3$ as $x \to 1$, and $V_\pi(x) \sim (1-x)$ as $x \to 1$. Comparing Figs. 2 and 3, we note that the region of x over which $R(x)$ appears to be decreasing monotonically ($0.05 < x < 0.55$) is a region in which the valence-quark component of $F_2^N(x)$ is rapidly gaining strength relative to the ocean component. This is the basis of the claim[2] that the data in Fig. 2 show that the momentum carried by valence quarks is reduced in a heavy nucleus from that observed in free nucleons.

For small x, we may fit the structure functions in Fig. 3 to exponential forms:

$$F_2^N(x) \simeq A_N \exp(-\lambda_N x) \quad (x < 0.4) \tag{2.24}$$

and

$$F_2^\pi(x) \simeq A_\pi \exp(-\lambda_\pi x) \quad (x < 0.2) \ . \tag{2.25}$$

We determine

$$A_N \simeq 0.45, \quad \lambda_N \simeq 3 \text{ to } 4 \ ,$$

and

$$A_\pi \simeq 0.42, \quad \lambda_\pi \simeq 4 \text{ to } 5 \ .$$

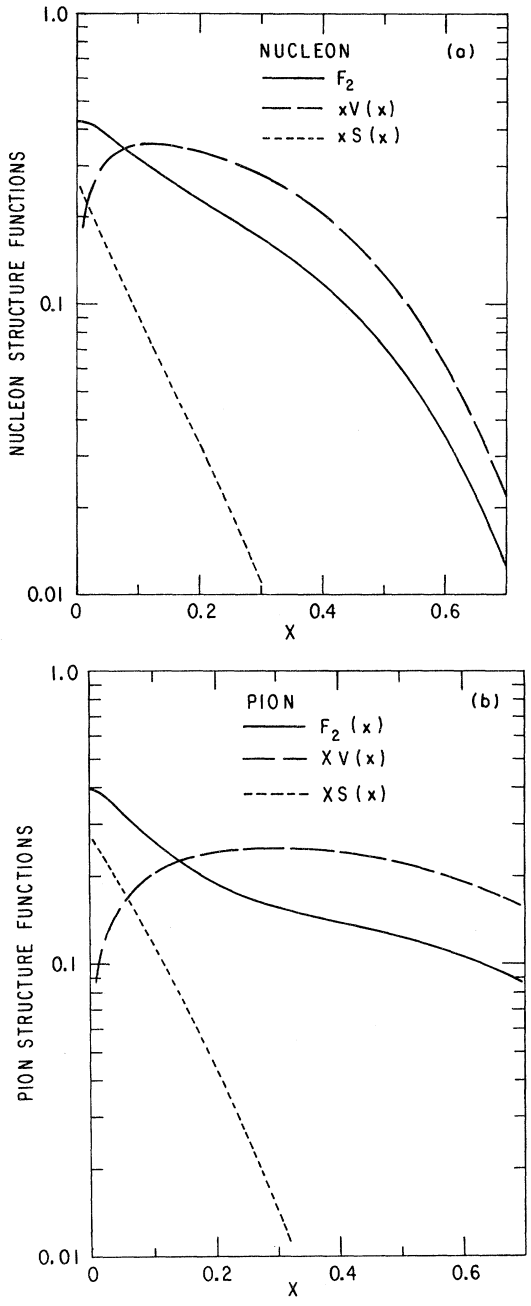

FIG. 3. (a) The structure function $F_2(x)$ for an isoscalar nucleon is shown as a solid line; the broad dashed curve denotes the valence distribution $xV(x)$, and the short dashed curve represents the ocean $xS(x)$. These curves are adapted from the CDHS nucleon structure functions (Ref. 8). (b) As in (a), but for the pion. These curves are derived from the CERN NA3 analysis (Ref. 10).

B. Empirical bounds on $\langle n_\pi \rangle$

Given values of $F_2^N(x)$ and $F_2^\pi(x)$ we can return to Eqs. (2.7)–(2.10) and try to establish bounds on $\langle n_\pi \rangle$, the effective number of excess pions per nucleon. We define a function

$$N_\pi(x) = \frac{F_2^N(x)}{F_2^\pi(x)}[R(x)-1] \ . \tag{2.26}$$

If we use for $R(x)$ the fit to the central values of the EMC data,[1] $R(x) = 1.18 - 0.52x$, and fit $N_\pi(x)$ to a linear form

for $0.05 < x < 0.3$, we obtain upon extrapolating to $x = 0$,

$$\langle n_\pi(\mathrm{Fe}) \rangle \geq 0.20 \ . \tag{2.27}$$

The lower bound is uncomfortably large, being roughly 1.5 times that obtained from the nuclear models discussed in Sec. IV. To achieve a smaller value of $\langle n_\pi \rangle$, one must try to increase $F_2^\pi(0)$ relative to $F_2^N(0)$. In the parton model, this would require increasing the momentum carried by the ocean constituents of the pion. In our parametrization, this momentum fraction is already a relatively large 18.3%, and the quarks plus antiquarks together carry 53% of the pion's momentum. In our view, any further increase in the momentum fraction carried by ocean constituents of the pion cannot be motivated on independent grounds. Indeed, modest variations of the pion quark and antiquark densities tend to reduce the value of $F_2^\pi(0)$ extrapolated to $x = 0$. For example, ignoring the massive-lepton-pair production data, one may be tempted to employ the constituent counting rules rigidly and write

$$xV_\pi(x) = \tfrac{3}{4}\sqrt{x}\,(1-x) \ , \tag{2.28}$$

along with

$$xS_\pi(x) = \frac{A_s'}{6}(p+1)(1-x)^p \ , \quad p = 7 \ . \tag{2.29}$$

In this case, the valence quarks carry 40% of the pion's momentum, an increase from the previous 35%. Choosing $A_s' = 0.1$, we would find that 50% of the pion's momentum is carried out by the quarks and antiquarks, leaving the remaining traditional 50% in the gluon field. In contrast to Fig. 3(b), the function $F_2^\pi(x)$ derived from Eqs. (2.28) and (2.29) shows no spike at small x. Fitting to the exponential form expressed in Eq. (2.25), we deduce $A_\pi' \simeq 0.22$ and $\lambda_\pi' \simeq 0.8$. From this alternative structure function we would extract $\langle n_\pi(\mathrm{Fe}) \rangle \gtrsim 0.38$ from the data, about twice the value of Eq. (2.27).

We summarize this subsection by remarking that the lower bound on the value of $\langle n_\pi \rangle$ extracted from the data is highly sensitive to the value of the ratio $F_2^N(x)/F_2^\pi(x)$ extrapolated to $x = 0$. The phenomenological bounds on this ratio are fairly broad, with unity being a rough lower limit and 2.0 being a rough upper bound. A quantitative fit to the central values of the EMC data in Fig. 2 requires $\langle n_\pi(\mathrm{Fe}) \rangle$ of at least 0.2; the value of 0.4 is not excluded. If we choose to fit only to the *lower* portion of the probable systematic error band shown in Fig. 2, we find $\langle n_\pi(\mathrm{Fe}) \rangle > 0.1$.

C. Slope of $R(x)$ at small x

The data[1] in Fig. 2 show that the ratio $R(x) = F_2^A(x)/F_2^N(x)$ decreases roughly linearly at small x. The slope $\partial R/\partial x$ is less sensitive to normalization uncertainties than is the intercept $R(0)$. In this subsection we derive an expression for $\partial R/\partial x$ from our model and show that its value at small x is very sensitive to the logarithmic derivatives of $F_2^N(x)$ and $F_2^\pi(x)$ at small x, as well as to $\langle n_\pi \rangle$.

From Eq. (1.1), we obtain

$$\frac{\partial F_2^A(x)}{\partial x} = \int_x \frac{dy}{y} f_\pi(y) \frac{\partial F_2^\pi\left[\frac{x}{y}\right]}{\partial\left[\frac{x}{y}\right]} + \int_x \frac{dz}{z} f_N(z) \frac{\partial F_2^N\left[\frac{x}{z}\right]}{\partial\left[\frac{x}{z}\right]} \tag{2.30}$$

We are interested in extracting some qualitative insight from Eq. (2.30) about the behavior of $\partial R/\partial x$ at small x. The second integrand poses no technical difficulties since $f_N(z)$ vanishes for small z. Because $f_\pi(y)$ is expected to peak for small values of y, the first integrands in Eqs. (1.1) and (2.30) will receive substantial contributions from a broad range of the argument (x/y) of F_2^π and its derivative. For this reason, the values of $R(x)$ and $\partial R(x)/\partial x$ in the interesting interval $0.05 < x < 0.5$ cannot be obtained readily from values of R and $\partial R/\partial x$ at exactly $x = 0$. Nevertheless, some important insight into the behavior of our function $R(x)$ is obtained by examining the $x = 0$ value of $\partial R/\partial x$. Using Eqs. (2.24) and (2.25), we find

$$\left.\frac{\partial R}{\partial x}\right|_{x\to 0} = \lambda_N \left[R(0) - \int_0 \frac{dz}{z} f_N(z) \right] - \lambda_\pi \frac{F_2^\pi(0)}{F_2^N(0)} \int_0 \frac{dy}{y} f_\pi(y) \ . \tag{2.31}$$

Equation (2.31) shows that the slope of $R(x)$ near $x = 0$ is influenced strongly by the logarithmic derivatives λ_N and λ_π of $F_2^N(x)$ and $F_2^\pi(x)$ at small x. While both or either may be quite small at some special value of Q^2, the (QCD) evolution of structure functions with Q^2 tends to increase these derivatives as Q^2 grows. From this point of view it is perhaps surprising that, in the data, the slope of $R(x)$ shows little variation with Q^2.

Some cancellation no doubt occurs between the two terms in the square brackets on the right-hand side of Eq. (2.31). Assuming exact cancellation, and approximating $\int (dy/y) f_\pi(y)$ crudely by $\langle n_\pi \rangle^2 / \langle y \rangle$, we obtain the estimate

$$\left.\frac{\partial R}{\partial x}\right|_{x\to 0} \simeq -\frac{\lambda_\pi \langle n_\pi \rangle}{\langle y \rangle} [R(0) - 1] \ . \tag{2.32}$$

We have invoked Eq. (2.6) in obtaining Eq. (2.32). Physical arguments associated with the relatively small values of m_π/m_N or of m_T/m_N, where $m_T^2 = \langle m_\pi^2 + p_T^2 \rangle$, suggest that $\langle y \rangle \simeq (0.2 \text{ to } 0.4) \langle n_\pi \rangle$. Thus, we estimate that $\partial R/\partial x$ near $x = 0$ should be in the neighborhood of $-\lambda_\pi$ or of $-\lambda_\pi/2$. Data[1] indicate that

$$\begin{aligned} &(\mathrm{Fe}) \ \frac{\partial R}{\partial x} = -0.52 \pm 0.04 \pm 0.21 \ (\mathrm{EMC}) \ , \\ &(\mathrm{Fe}) \ \frac{\partial R}{\partial x} \simeq -0.45 \pm 0.08 \ (\mathrm{SLAC}) \ , \\ &(\mathrm{Al}) \ \frac{\partial R}{\partial x} \simeq -0.30 \pm 0.06 \ (\mathrm{SLAC}) \ . \end{aligned} \tag{2.33}$$

These experimental slopes are about a factor of 4 to 10 smaller than we would expect near $x = 0$. The only way

we can accommodate such small slopes is to reduce λ_π considerably and/or to arrange for substantial cancellation between the two terms in Eq. (2.31). Reducing λ_π requires reducing the pion ocean contribution in $F_2^\pi(x)$ at small x and, perhaps, arranging a careful compensation between the valence and ocean contributions in Fig. 3. While this could conceivably be done at one value of Q^2, the evolution of structure functions with Q^2 would perhaps lead to rapid changes of $\partial R/\partial x$ with Q^2, not observed in the data. Moreover, any reduction of the pion ocean contribution to achieve a smaller λ_π, would force a compensating increase in $\langle n_\pi \rangle$ in order to maintain an acceptable value of the intercept $R(0)$.

We repeat that the large value derived here for $\partial R/\partial x$ is appropriate only very near $x=0$. Our numerical work discussed in Sec. II D and in Sec. IV shows that the theoretical slope decreases as x enters the interesting range $0.05<x<0.5$ in which there are data. Our theoretical $R(x)$ is not at all well represented by the simple linear form $R(x)=R(0)(1-cx)$. Nevertheless, the lesson of the analysis of this subsection is that our theoretical $R(x)$ will decrease very rapidly as x is increased away from $x=0$. If we adjust our theoretical $R(x)$ to yield the value $R_{\text{expt}}(0)$ obtained from the simple linear extrapolation described in Sec. II B, then our values for $R(x)$ in the range $0.05<x<0.3$ will necessarily fall considerably below the data. Boosting our theoretical $R(0)$ sufficiently may allow our function $R(x)$ to pass through the data in the region $x\simeq 0.1$. However, barring a large increase of $F_2^\pi(0)$, which we consider unacceptable, increasing $\langle n_\pi \rangle$ is the only mechanism we have for increasing $R(0)$. *A fit to both the intercept and the slope of $R(x)$ seems impossible to achieve in the context of known constraints on $F_2^\pi(x)$ and the relatively small values of $\langle n_\pi \rangle$ suggested by nuclear models.* We note in passing that the successful description of the data achieved by Ericson and Thomas[5] may be associated with their assumption that $F_2^\pi(x)$ is a constant ($\lambda_\pi=0$) for $x\lesssim 0.3$. We do not believe this assumption is a fair representation of the information available on $F_2^\pi(x)$, discussed in Sec. II A.

In summary, the value of the slope of $R(x)$ in the interesting region $0.05<x<0.4$ is influenced strongly by three effects: (i) the value of $\langle n_\pi \rangle$, (ii) the values of $F_2^\pi(x)$ and $F_2^N(x)$, and (iii) momentum balance between the mesons and nucleons in the nucleus.

D. Toy model

From the detailed nuclear models studied in Secs. III and IV, we shall derive explicit functional forms for the functions $f_\pi(y)$ and $f_N(z)$ which represent the probabilities to find mesons and nucleons carrying fractional longitudinal momenta y and z. In this subsection we preempt some of those results by postulating a simple *ad hoc* form for $f_\pi(y)$, and imposing momentum balance in the simplest manner possible to derive $f_N(z)$ from $f_\pi(y)$.

We choose to parametrize $f_\pi(y)$ as

$$f_\pi(y)=\langle n_\pi \rangle \frac{\Gamma(a+b+2)}{\Gamma(a+1)\Gamma(b+1)} y^a(1-y)^b , \tag{2.34}$$

$0\le y\le 1$. The parameters a and b may be varied so as to alter the y dependence of $f_\pi(y)$. We note that

$$\langle y \rangle \equiv \int_0^1 y f_\pi(y)dy = \frac{(a+1)}{(a+b+2)} \langle n_\pi \rangle . \tag{2.35}$$

For conceptual simplicity we find it convenient to associate the pions with nucleons, on a one to one basis. We picture the nucleus as a collection of nucleon and of nucleon-pion subsystems. We neglect any difference in the effective masses of the nucleon and nucleon-pion subsystems as well as the Fermi motion of these subsystems relative to one another. Thus, in a nucleus of large longitudinal momentum P, each subsystem carries longitudinal momentum P/A. This approximation should be adequate so long as x is not too near its maximum (i.e., $x\lesssim 0.6$). In $\mu A\to\mu' X$, the exchanged virtual photon may interact with a "free" nucleon in the nucleus, with probability $(1-\langle n_\pi \rangle)$, or with either the pion *or* the nucleon of the nucleon-pion system. The nucleon in the subsystem carries longitudinal momentum fraction $(1-y)$, with probability $f_\pi(y)$. Thus, we derive immediately

$$f_N(z)=(1-\langle n_\pi \rangle)\delta(z-1)+f_\pi(1-z) , \tag{2.36}$$

and, in our toy model, Eq. (1.1) becomes

$$\begin{aligned} F_2^A(x)=&(1-\langle n_\pi \rangle)F_2^N(x) \\ &+\int_x^1 dy\, f_\pi(y)F_2^\pi(x/y) \\ &+\int_x^1 dz\, f_\pi(1-z)F_2^N(x/z) . \end{aligned} \tag{2.37}$$

We note that in this approach any enhancement of $F_2^A(x)$ at small x associated with the enhanced pion cloud will be compensated to some degree by a depletion of $F_2^A(x)$ at larger x. This effect, also observed in the data, arises here from momentum conservation. The structure function $F_2(x)$ probes the momentum distribution of the constituents; momentum carried by the extra pions is removed from nucleons.

We have investigated the results obtained for $R(x)$ for a fairly broad range of the parameters a and b in Eq. (2.34). Selecting $\langle n_\pi \rangle=0.22$, consistent with the bound in Eq. (2.27), and using the structure functions defined in Sec. II B, we obtain the results shown in Fig. 4(a). These results were obtained with the choices $a=1$ and $b=3$, which provide $\langle y \rangle=\langle n_\pi \rangle/3$. Very similar results are obtained with the parameter set $(a,b)=(2,5)$ which preserves $\langle y \rangle$.

In Fig. 4(a), we show the total result $R(x)$ and the contribution from the pion term alone,

$$\Delta R_\pi(x)\equiv \int_x^1 dy\, f_\pi(y)F_2^\pi(x/y)\Big/F_2^N(x) . \tag{2.38}$$

Both $R(x)$ and $\Delta R_\pi(x)$ show the sharp decrease for $x<0.05$ discussed in Sec. II C. In the region $0.05<x<0.5$, the slope of our calculated $R(x)$ is in fine agreement with the slope of the experimental $R(x)$. However, the theoretical curve is everywhere about 0.05 units below the data.

A comparison of the two curves in Fig. 4(a) indicates that the nucleon contributions are important even in the region of small x. This effect arises from momentum balance between the mesons and the nucleons, and it is not an

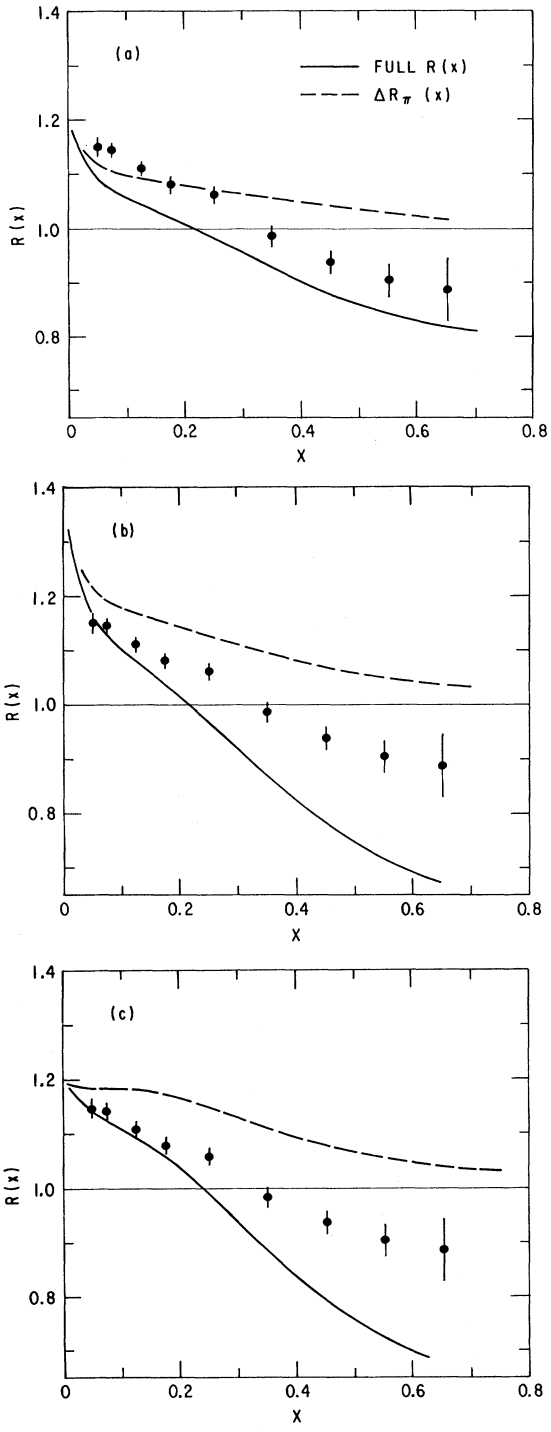

FIG. 4. Comparison of our theoretical $R(x)=F_2^A(x)/F_2^N$ with the EMC data of Ref. 1. The solid curve shows the full result of the "toy model" described in Sec. II D, whereas the dashed curve represents $\Delta R_\pi(x)$, the contribution to $R(x)$ of scattering from the constituents of the mesons. In (a), we set $\langle n_\pi\rangle=0.22$, $\langle y\rangle=\langle n_\pi\rangle/3$, and we use the CDHS nucleon structure functions and the NA3 pion structure functions, both evaluated at $\langle Q^2\rangle=25$ GeV^2; (b) as in (a), except that $\langle n_\pi\rangle=0.4$; (c) as in (a), except that $\langle n_\pi\rangle=0.4$, and for the pion, we use the simple parton model structure functions of Eqs. (2.28) and (2.29).

artifact of the simplistic method chosen in this subsection for achieving that balance. Essentially identical results below $x=0.4$ are obtained if we use the more sophisticated method discussed in Sec. IV. It is therefore inappropriate[5] to compare only $\Delta R_\pi(x)$ with the data. Even at small x, such a comparison neglects important (negative) effects associated with the degradation of the momentum of the nucleons.

In an attempt to achieve better agreement with the data we tried varying $\langle y\rangle$ over the interval $\langle n_\pi\rangle/6$ to $\langle n_\pi\rangle/2$, to little avail. Retaining $\langle y\rangle=\langle n_\pi\rangle/3$, and boosting $\langle n_\pi\rangle$ to 0.4, we obtain the results shown in Fig. 4(b). The agreement with the data below $x=0.1$ is achieved at the price of substantial disagreement for $x>0.3$. The slope of our theoretical $R(x)$ no longer parallels that of the data. The value $\langle n_\pi\rangle=0.4$ is also more than a factor of 3 greater than predicted in nuclear models, as described in Sec. IV.

Finally, recalling our analysis of $\partial R/\partial x$ in Sec. II C, we considered altering the pion structure function $F_2^\pi(x)$ to one with a smaller logarithmic derivative λ_π at $x=0$. Changing to the naive parton model form specified in Eqs. (2.28) and (2.29) (whose $\lambda_\pi\simeq 0.8$), and retaining $\langle n_\pi\rangle=0.4$, we obtain the results shown in Fig. 4(c). The agreement with the data is respectable for $x<0.2$; the discrepancy at larger x is a direct consequence of the very large value of $\langle n_\pi\rangle$ required to fit data in the small x region.

The conclusions of this subsection are reinforced by the analysis carried out with nuclear models for $f_\pi(y)$ in Sec. IV. The magnitude of the central values of the data on $R(x)$ at small x cannot be reproduced within the context of the approach studied in this paper unless we select *ad hoc* values of $\langle n_\pi\rangle$ as large as 0.4. Such large values of $\langle n_\pi\rangle$ are incompatible with nuclear models and result in inevitable serious discrepancies with the data on $R(x)$ at intermediate values of x $(0.2<x<0.5)$. These conclusions are insensitive to the methods we have explored to enforce momentum balance between the meson and nucleon constituents of the nucleus. If we redefine our goal to be that of reproducing only the *slope* of $R(x)$ in the region $0.05<x<0.5$, we can achieve a good match to the data if we use the structure functions of Sec. II B and values of $\langle n_\pi\rangle$ compatible with nuclear models.

III. CALCULATION OF STRUCTURE FUNCTIONS OF COMPOUND SYSTEMS

In this section we calculate the structure functions of compound systems, whose constituents are themselves not structureless, in terms of the structure functions of the constituents and the wave functions of the compound system. We establish that this can always be done consistent with the requirements of Lorentz invariance and the principles of quantum mechanics.[13] The structure function of the compound system shall be shown to be a linear functional of the structure functions of the constituents. It can be obtained for any value of the momentum transfer, but is especially simple for large Q^2. In practice nuclear wave functions are, of course, nonrelativistic. However, they can be understood as low velocity approximations of

relativistic wave functions. The validity of this approximation is independent of the velocity of the nucleus as a whole and depends only on the smallness of the velocities of nucleons relative to their center of mass.

The structure function $F_2(x,Q^2)$ is defined in terms of matrix elements of the target current by

$$F_2=F^{\mu\nu}[\tfrac{3}{2}\tilde{p}_\mu\tilde{p}_\nu/(-\tilde{p}^2)+\tfrac{1}{2}g_{\mu\nu}](p\cdot Q)/(-\tilde{p}^2)\ , \tag{3.1}$$

where p is the initial momentum of the target, and

$$\tilde{p}=p-(p\cdot Q)Q/Q^2\ . \tag{3.2}$$

The tensor $F^{\mu\nu}$ depends on the matrix elements of the current density in the target,

$$F^{\mu\nu}=\int d^3p'\sum_\alpha\sum_{S'm_S'}\frac{1}{2S+1}\sum_S\delta(p'-p-Q)\langle\vec{p}\,',\alpha,S',m_S'\,|\,j^\mu(0)\,|\,\vec{p},m_S\rangle\langle\vec{p}\,',\alpha,S',m_S'\,|\,j^\nu(0)\,|\,\vec{p},m_S\rangle^*E\ , \tag{3.3}$$

where $E=(\vec{p}^{\,2}+M^2)^{1/2}$, and the states $|\,\vec{p},m_S\rangle$ are normalized according to

$$\langle m_S',S',\vec{p}\,'\,|\,\vec{p},S,m_S\rangle=\delta(\vec{p}\,'-\vec{p})\delta_{S,S'}\delta_{m_S,m_S'}\ . \tag{3.4}$$

Symbols S, m_S stand for spin, and α represents all other quantum numbers; M is the mass of the target.

The properties of relativistic wave functions representing the state vector of the target can be formulated conveniently in terms of suitably defined functions of the momenta of the particles. Let $p_1,\ldots,p_N$ be the momenta of N particles of mass m, $p_i^2=-m^2$, and define

$$P=\sum_i p_i,\quad |P|=(-P^2)^{1/2}\ , \tag{3.5}$$

$$p_{i\perp}=p_i-(p_i\cdot P)P/P^2,\quad \kappa_i=-(p_i\cdot P)/|P|\ . \tag{3.6}$$

From these definitions it follows that

$$\sum_i p_{i\perp}=0\ ,\quad \sum_i\kappa_i=|P|\ ,\quad \kappa_i=(p_{i\perp}^2+m^2)^{1/2}\ . \tag{3.7}$$

Let $L(P)$ be the Lorentz boost with the defining property $L(P)P=\{|P|,\vec{0}\}$. Because the time component of the vector $L(P)p_{i\perp}$ vanishes, we can define the momenta $\vec{q}_i$ as functions of $p_1,\ldots,p_N$ by

$$\{0,\vec{q}_i\}=L(P)p_{i\perp}\ . \tag{3.8}$$

Since $\vec{q}_i\cdot\vec{q}_j=p_{i\perp}\cdot p_{ij\perp}$, scalar functions of the $\vec{q}$'s are Lorentz invariant. The three-vectors $\vec{q}$ are defined in any frame, but, loosely speaking, are the relative momenta in the center-of-mass frame.

Bound-state wave functions for a compound system of spin zero are therefore scalar functions $\chi(q_1,\ldots,q_N)$. They satisfy an eigenvalue equation of the general form

$$(|P|+v)\chi=\chi M\ , \tag{3.9}$$

and have the Hilbert-space norm

$$||\chi||^2=\int d^3q_1\cdots\int d^2q_N\,|\chi(\vec{q}_1,\ldots,\vec{q}_N)|^2\delta\left(\sum_i\vec{q}_i\right)$$
$$=1\ . \tag{3.10}$$

Here M is the mass of the bound system, and v is some invariant interaction operator.

For nonzero spin the bound-state wave functions transform under rotations in the same way as nonrelativistic wave functions; densities averaged over spin components are again Lorentz invariant. We suppress the spin variables of the constituent particles in this discussion, since they introduce no significant problems. The wave functions χ do not give a complete description of the nucleus since they do not include a representation of the center-of-mass motion. Relativity and quantum theory require that there be a unitary representation $U(\Lambda)$ of the Lorentz transformations Λ such that current density operators $j^\mu(x)$ and state vectors $|\,\vec{p},S,m_S\rangle$ satisfy the covariance relations

$$U(\Lambda)j^\mu(x)U^{-1}(\Lambda)+\Lambda^\mu_\nu j^\nu(\Lambda^{-1}x)\ , \tag{3.11}$$

$$U(\Lambda)\,|\,\vec{p},S,m_S\rangle$$
$$=\sum_{m_S'}|\,\hat{\vec{p}},Sm_S'\rangle D^S_{m_S',m_S}(R(\Lambda,p))(\hat{E}/E)^{1/2}\ , \tag{3.12}$$

where $R(\Lambda,p)=L(\hat{p})\Lambda L^{-1}(p),\hat{p}=\Lambda p$.

For a consistent calculation of structure functions it is sufficient to achieve covariance of the state vectors under Lorentz boosts in one direction, namely, the direction of the momentum transfer $\vec{Q}$ in the rest frame of the target. This requirement can be imposed explicitly on the wave function. Let $\vec{n}$ be a unit vector in the direction of $\vec{Q}$ in the rest frame of p, and define "light-front" components P_+, P_-, and $\vec{P}_T$ by

$$P_+=\vec{P}\cdot\vec{n}+(\vec{P}^{\,2}+|P|^2)^{1/2}\ , \tag{3.13}$$

$$\vec{P}_T=\vec{P}-(\vec{n}\cdot\vec{P})\ , \tag{3.14}$$

$$P_-=-(|P|^2+\vec{P}_T^{\,2})/P_+\ . \tag{3.15}$$

Corresponding components are defined for any four vector. The desired wave function with manifest light-front symmetry is then

$$\Psi_p(\vec{p}_{1T},\ldots,\vec{p}_{NT};p_{1+},\ldots,p_{N+})$$
$$=J^{1/2}\chi(\vec{q}_1,\ldots,\vec{q}_N)\delta(\vec{P}_T-\vec{P}_T)\delta(P_+-p_+)\ , \tag{3.16}$$

where J is the appropriate Jacobian.

The light-front momentum fraction x_i,

$$x_i=p_{i+}/P_+\ , \tag{3.17}$$

is invariant under boosts in the direction $\vec{n}$. For $\vec{P}_T=0$, x_i is related to the $\vec{q}$'s by

$$x_i=p_{i+}/P_+=(\vec{n}\cdot\vec{q}_i+\kappa_i)/|P| \tag{3.18}$$

(obtained by evaluating numerator and denominator in the frame in which $P_+=|P|$). It is therefore a straightforward change of variables to express the wave function χ as a function of the new variables $\vec{q}_{1T},\ldots,\vec{q}_{NT}$; $x_1,\ldots,x_N$. The Hilbert-space norm $||\chi||$ is then

$$||\chi||^2=\int d^2q_{1T}\cdots\int d^2q_{NT}\int dx_1\cdots\int dx_N\,|\chi(\vec{q}_{1T},\ldots,\vec{q}_{NT};x_1,\ldots,x_N)|^2\delta\left[\sum_i x_i-1\right]\delta\left[\sum_i\vec{q}_{iT}\right]. \tag{3.19}$$

For a nucleus with A nucleons and a variable number of pions we have wave functions $\chi_n(\vec{q}_1,\ldots,\vec{q}_A,\vec{k}_1,\ldots,\vec{k}_n)$ with the normalization

$$\sum_n\int d^3q_1\cdots\int d^3q_A\int d^3k_1\cdots\int d^3k_n\,|\chi_n(\vec{q}_1,\ldots,\vec{q}_A,\vec{k}_1,\ldots,\vec{k}_n)|^2\delta\left[\sum_i\vec{q}_i+\sum_j\vec{k}_j\right]=1\,. \tag{3.20}$$

The corresponding momentum distributions $\rho_N(\vec{q})$ and $\rho_\pi(\vec{k})$ of nucleons and pions are

$$\rho_N(\vec{q})=\sum_n\int d^3q_1\cdots\int d^3q_A\int d^3k_1\cdots\int d^3k_n\delta(\vec{q}-\vec{q}_1)\delta\left[\sum_i\vec{q}_i+\sum_j\vec{k}_j\right]|\chi_n(q_1,\ldots,q_A;k_1,\ldots,k_n)|^2\,, \tag{3.21}$$

$$\rho_\pi(\vec{k})=\sum_n\frac{n}{A}\int d^3q_1\cdots\int d^3q_A\int d^3k_1\cdots\int d^3k_n\delta(\vec{k}-\vec{k}_1)\delta\left[\sum_i\vec{q}_i+\sum_j\vec{k}_j\right]|\chi_n(q_1,\ldots,q_A;k_1,\ldots,k_n)|^2\,. \tag{3.22}$$

Instead of these densities which are functions of $\vec{k}$ and $\vec{q}$, we need, for our purposes, densities that are functions of the light-front momentum fractions y and z of the pions and nucleons. So that we may discuss momentum fractions per nucleon, it is convenient to introduce a factor A into the definitions

$$z_i=A\frac{p_{i+}}{P_+}=A\frac{\vec{n}\cdot\vec{q}_i+(\vec{q}_i^{\,2}+m_N^2)^{1/2}}{|P|} \tag{3.23}$$

and

$$y_j=A\frac{p_{\pi j+}}{P_+}=A\frac{\vec{n}\cdot\vec{k}_j+(\vec{k}_j^{\,2}+m_\pi^2)^{1/2}}{|P|}\,, \tag{3.24}$$

where P is again the total momentum

$$P=\sum_i p_i+\sum_j p_{\pi j}\,. \tag{3.25}$$

It follows that

$$\sum_i z_i+\sum_j y_j=A\,. \tag{3.26}$$

Joint probability distributions $f_n(z_1,\ldots,z_A,y_1,\ldots,y_n)$ are defined as the squares of the wave functions integrated over all transverse momenta. Integrating over all but one constituent, we obtain the momentum distributions of the pions and nucleons,

$$f_\pi(y)=\sum_n\int dz_1\cdots\int dz_A\int dy_1\cdots\int dy_n\delta(y-y_1)\delta\left[\sum z_i+\sum y_j-A\right]\frac{n}{A}f_n(z_1,\ldots,z_A;y_1,\ldots,y_n) \tag{3.27}$$

and

$$f_N(z)=\sum_n\int dz_1,\ldots,\int dz_A\int dy_1,\ldots,\int dy_n\delta(z-z_1)\delta\left[\sum z_i+\sum y_j-A\right]f_n(z_1,\ldots,z_A;y_1,\ldots,y_n)\,. \tag{3.28}$$

From these definitions and Eq. (3.26) follows the important momentum-balance relation

$$\int dz\,zf_N(z)+\int dy\,yf_\pi(y)=1\,, \tag{3.29}$$

while

$$\int dz\,f_N(z)=1\text{ and }\int dy\,f_\pi(y)=\langle n_\pi\rangle\,. \tag{3.30}$$

If we assume that the pions and nucleons in the nucleus contribute incoherently, then the structure function F_2^A per nucleon of the nucleus is a linear functional of the nucleon and pion structure functions F_2^N and F_2^π,

$$F_2^A(x,Q^2)=A\left[\int dz\, F_2^N\left[\frac{x}{z}\right]\frac{(p\cdot Q)}{z(p_N\cdot Q)}\left[\frac{3}{2}\frac{(\tilde{p}_N\cdot\tilde{p})^2}{\tilde{p}^4}-\frac{1}{2}\frac{\tilde{p}_N{}^2}{\tilde{p}^2}\right]f_N(z)\right]$$

$$+A\left[\int dy\, F_2^\pi\left[\frac{x}{y}\right]\frac{(p\cdot Q)}{y(p_\pi\cdot Q)}\left[\frac{3}{2}\frac{(\tilde{p}_\pi\cdot\tilde{p})^2}{\tilde{p}^4}-\frac{1}{2}\frac{\tilde{p}_\pi{}^2}{\tilde{p}^2}\right]f_\pi(y)\right], \tag{3.31}$$

where $\tilde{p}=p-(p\cdot Q)Q/Q^2$. For $Q^2\gg m_N{}^2$, Eq. (3.31) reduces to

$$F_2^A(x)=\int dz\, F_2^N\left[\frac{x}{z}\right]f_N(z)+\int dy\, F_2^\pi\left[\frac{x}{y}\right]f_\pi(y)\ . \tag{3.32}$$

If $A=1$ and $n=0,1$ Eqs. (3.27), and (3.28) become

$$f_\pi(y)=\int dz\, f_1(z,y)\delta(z+y-1) \tag{3.33}$$

and

$$f_N(z)=f_0\delta(z-1)+\int dy\, f_1(z,y)\delta(z+y-1)$$
$$=(1-\langle n_\pi\rangle)\delta(z-1)+f_\pi(1-z)\ . \tag{3.34}$$

If we assume that the nucleus is a collection of individual dressed nucleons with each pion cloud modified by the medium, and neglect the Fermi motion of the nucleons, then we recover the toy model of the last section. In that case Eq. (3.24) becomes

$$y=\frac{\vec{n}\cdot\vec{k}+(\vec{k}^2+m_\pi{}^2)^{1/2}}{(\vec{k}^2+m_\pi{}^2)^{1/2}+(\vec{k}^2+m_N{}^2)^{1/2}} \tag{3.35}$$

and $f_\pi(y)$ can be calculated from Eq. (3.35) provided we have a theory for the modification by the medium of the pion clouds of single nucleons. In this paper we will not pursue this avenue further.

IV. APPROXIMATE CALCULATIONS OF NUCLEON AND PION MOMENTUM DISTRIBUTIONS

In this section we discuss the approximations we make in obtaining $\rho_N(\vec{q})$, $\rho_\pi(\vec{k})$, $f_N(z)$, and $f_\pi(y)$. The momentum densities $\rho_\pi(\vec{k})$ and $\rho_N(\vec{q})$ are readily accessible in terms of conventional nuclear theory. The developments of Sec. III show that $f_N(z)$ and $f_\pi(y)$ can in principle be calculated from ordinary nuclear wave functions, but there are no exact relations between the momentum densities $\rho_N(\vec{q})$ and $\rho_\pi(\vec{k})$ and the functions $f_N(z)$, $f_\pi(y)$. In this paper we obtain approximate forms for $f_\pi(y)$ and $f_N(z)$ by relating them to the densities $\rho_\pi(\vec{k})$ and $\rho_N(\vec{q})$. These approximate relations should be adequate at least for an initial orientation. The approximation consists of redefining the momentum fractions z and y by

$$z=A[\vec{n}\cdot\vec{q}+(\vec{q}^2+m_N{}^2)^{1/2}]/\langle\,|P|\,\rangle\ , \tag{4.1}$$

$$y=A[\vec{n}\cdot\vec{k}+(\vec{k}^2+m_\pi{}^2)^{1/2}]/\langle\,|P|\,\rangle\ . \tag{4.2}$$

The replacement of $|P|$ by $\langle\,|P|\,\rangle$ allows us to remove $\langle\,|P|\,\rangle$ from the integrand. The densities $f_N(z)$ and $f_\pi(y)$ can then be obtained from $\rho_N(\vec{q}_T,z)$ and $\rho_\pi(\vec{k}_T,y)$ by integrating over the transverse momenta. Equations (4.1) and (4.2) are designed to maintain the momentum balance Eq. (3.29).

The nuclear bound-state wave functions $\chi_n(\vec{q}_1,\ldots,\vec{q}_A;\vec{k}_1,\ldots,\vec{k}_n)$, $n=0,1,\ldots$, are eigenfunctions of a Hamiltonian of the general form

$$H=H_N+\int d^3k\, c_\pi^\dagger(\vec{k})c_\pi(\vec{k})\omega_\pi(\vec{k})+H'\ , \tag{4.3}$$

where H_N acts only on the nucleon coordinates $\omega_\pi=(\vec{k}^2+m_\pi{}^2)^{1/2}$ and the interaction term H',

$$H'=(2\pi)^{-3/2}f\int d^3k\int d^3p'\int d^3p\,\delta(\vec{p}\,'+\vec{k}-\vec{p})[(\Lambda^2-m_\pi{}^2)/(\vec{k}^2+\Lambda^2)]^2/m_\pi$$
$$\times\sum_\rho c_N^\dagger(\vec{p}\,')i\vec{\sigma}\cdot\vec{k}\tau_\rho c_N(\vec{p})[c_{\pi\rho}^\dagger(\vec{k})+c_{\pi\rho}(-\vec{k})]/(2\omega_\pi)^{1/2} \tag{4.4}$$

creates and annihilates pions. The operators $c_N^\dagger(\vec{p}\,'),c_N(\vec{p})c_\pi^\dagger(\vec{k}),c_\pi(\vec{k})$ are nucleon and pion creation and annihilation operators; $f^2/4\pi=0.08$; $\Lambda=7$ fm^{-1}; $\vec{\sigma}$ and τ_ρ are spin and isospin matrices.

The standard procedure in nuclear theory is to eliminate the functions χ_n for $n>0$ from the Schrödinger equation and the normalization condition (3.20). The nucleon momentum density $\rho_N(\vec{q})$ is then

$$\rho_N(\vec{q})=\int d^3q_1\cdots\int d^3q_A\,\delta(\vec{q}-\vec{q}_1)\delta$$
$$\times\left[\sum_i\vec{q}_i\right]|\chi_0(\vec{q}_1,\ldots,\vec{q}_A)|^2\ . \tag{4.5}$$

It should be adequate for our purposes to approximate the momentum distribution in a nucleus by that of homogeneous nuclear matter at a representative density.[14] In that case $\rho_N(\vec{q})$ is constant if $|\vec{q}|$ is less than the Fermi momentum k_F. The high-momentum tail, $|\vec{q}|>k_F$, of the momentum distribution contains only about 11% of the nucleons.[15] In calculating $f_N(z)$ with Eq. (4.1) we will neglect the high-momentum tail as a matter of convenience. We have included the tail in a sample calculation and verified that its numerical effect on the ratio $R(x)$ is negligible for $x\lesssim 0.5$. For an uncorrelated Fermi gas the function $f_N(z)$ obtained from Eq. (4.1) is well approximated by the expression

$$f_N(z)=\alpha\tfrac{3}{4}(m_N/k_F)^3[(k_F/m_N)^2-\tfrac{1}{4}(\alpha z-1/\alpha z)^2]\ , \tag{4.6}$$

for

$$(k_F^2+m_N^2)^{1/2}-k_F\le\alpha z m_N\le(k_F^2+m_N^2)^{1/2}+k_F;$$

$$\alpha=\langle\,|P|\,\rangle/Am_N\ .$$

Outside this range, $f_N(z)$ vanishes. We have used $k_F=1.08$, 1.13, and 1.23 fm^{-1}, respectively, for Al, Fe, and Pb.

The pion momentum distribution $\rho_\pi(\vec{k})$ is related to the expectation value of the pion number operator by

$$\rho_\pi(\vec{k})=\frac{1}{A}\langle\,|c^\dagger(\vec{k})c(\vec{k})|\,\rangle\ , \tag{4.7}$$

where $|\,\rangle$ is the state vector represented by the wave functions χ_n. Since we wish to identify $F_2^N(x)$ with the measured structure function of an isolated nucleon, including the effects of its pion cloud, we must extract the excess density $\rho_{\pi,\mathrm{ex}}(\vec{k})$ due to meson exchange from the total pion density $\rho_\pi(\vec{k})$. We use conventional methods of nuclear potential calculations for separating the effects of the pion clouds of single nucleons from medium-dependent effects.[16–18] The pionic self-energy of the nucleons is absorbed in the nucleon mass while the medium-dependent energy is the expectation value of the pion-exchange potentials. The same procedure is applicable to other quantities since the ground-state expectation value of any operator can be formally obtained as the linear response of the energy to a perturbation of the Hamiltonian. With

$$H(\eta)=H_N+\int d^3k'c^\dagger(\vec{k}')c(\vec{k}')\times[\omega_\pi(\vec{k}')+\eta\delta(\vec{k}-\vec{k}')]+H'\ , \tag{4.8}$$

we have obviously

$$\rho_\pi(\vec{k})=\frac{1}{A}\left[\frac{d\langle\,|H(\eta)|\,\rangle}{d\eta}\right]_{\eta=0}\ . \tag{4.9}$$

This remark points to the way in which we can extract excess pion densities. The interaction H' is responsible both for the pion self-energy of isolated nucleons and the pion exchange that provides the long- and medium-range attraction between nucleons. The self-energy is, of course, eliminated from calculations of nuclear binding energies. Using Eq. (4.9) we can eliminate the pion clouds of isolated nucleons and thus find a formula for the excess pion momentum distribution associated with one-pion exchange (OPE),[16,17]

$$\rho_{\pi,\mathrm{ex}}(\vec{k})=-\langle\,|\omega_\pi^{-1}V_{\mathrm{OPE}}(\vec{k})|\,\rangle\frac{1}{A}\ . \tag{4.10}$$

For consistency it is important that the potential used in the above pion-density operator be the same as that used to calculate the wave functions. In order to include in a convenient manner at least a substantial fraction of the two-pion exchange effects we include Δ isobar states of the nucleons and use a Hamiltonian which includes $N\Delta\pi$ and $\Delta\Delta\pi$ vertices.[18] We see from Eq. (4.10) that the excess pion density is opposite in sign to the contribution $\langle\,|V_{\mathrm{OPE}}(\vec{k})|\,\rangle$ to the potential energy. In nuclear systems $\langle\,|V_{\mathrm{OPE}}(\vec{k})|\,\rangle$ is positive for small $|k|$, so the medium decreases the pion density, i.e., the excess pion density is negative for small $|\vec{k}|$. This can be understood as a result of Pauli blocking on the nucleon's pion cloud. For larger $|\vec{k}|$, $\langle\,|V_{\mathrm{OPE}}(\vec{k})|\,\rangle$ is negative, providing the nuclear binding, and the excess pion density is consequently positive.[16]

In this manner we have obtained $\rho_{\pi,\mathrm{ex}}(\vec{k})$ for deuterium and for homogeneous nuclear matter of different densities. For aluminum, iron, and lead we have averaged nuclear-matter results over the appropriate nucleon densities.[19] The results are shown in Fig. 5. The pion momentum distributions for aluminum, iron, and lead are very similar to those obtained for homogeneous nuclear matter at $k_F=1.08$, 1.13, and 1.23 fm^{-1}, respectively. We find that $\langle n_\pi\rangle=0.025$, 0.119, 0.126, and 0.142 for D, Al, Fe, and Pb, respectively. We note that $\langle n_\pi\rangle$ increases rapidly with A for small values of A, then tends to level off.[16] Qualitatively, this implies that both the slope of $R(x)$ and its extrapolated intercept at $x=0$ should also increase rapidly for low values of A but then show little change with A for $A\gtrsim$ Al.

The corresponding light-front momentum distribution $f_\pi(y)$ for iron, obtained from the use of Eq. (4.2), is denoted in Fig. 6 by a solid line. In Fig. 7(a) we present the ratio $R(x)$ calculated from Eq. (1.1) using this pion distribution and the pion structure function shown in Fig. 3(b). The average slope of $R(x)$ follows that of the data, but the magnitude of $R(x)$ is too small, particularly at small x. We find that changing to the simple parton model structure functions of Eqs. (2.28) and (2.29) makes no significant difference, except for $x<0.05$. In view of the uncertainty involved in the approximations (4.2) we have investigated the effect of scale transformations on y that alter $\langle y\rangle$ without changing the number of pions per nucleon. The number of pions per nucleon can be changed independently. We find that the slope of the ratio $R(x)$ can be reproduced quite accurately; but not the magnitude. As $\langle y\rangle$ is decreased, the theoretical $R(x)$ diminishes at small x ($x=0.05$ to 0.15) and increases at larger x ($x\cong0.5$). Increasing $\langle n_\pi\rangle$ with $\langle y\rangle$ fixed, raises $R(x)$ at small x and

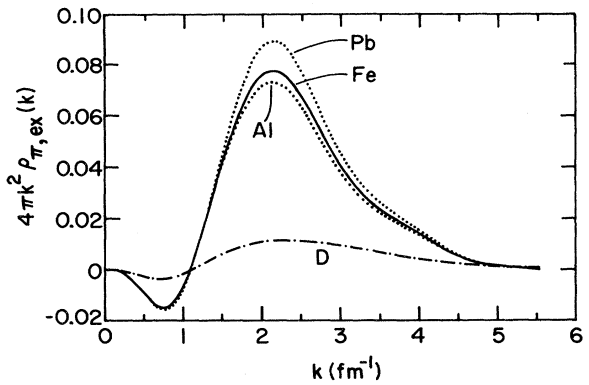

FIG. 5. The densities $4\pi k^2\rho_{\pi,\mathrm{ex}}(\vec{k})$ vs $\vec{k}$ for Pb, Fe, Al, and D. These are normalized such that $\int d^3k\,\rho_{\pi,\mathrm{ex}}(\vec{k})=\langle n_\pi\rangle$.

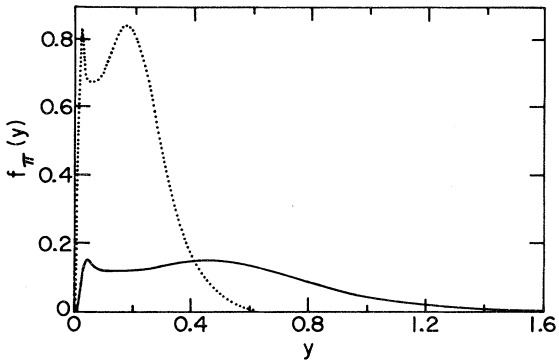

FIG. 6. The functions $f_\pi(y)$ for Fe obtained from $\rho_\pi(\vec{k})$ shown in Fig. 5 by the methods described in Sec. IV. For the solid curve, $\langle n_\pi \rangle = 0.126$ and $\langle y \rangle = 0.065$; for the dotted curve, $\langle n_\pi \rangle = 0.252$ and $\langle y \rangle = 0.047$.

depresses it near $x=0.5$. The distribution shown by a dashed line in Fig. 6 is obtained by doubling the pion number and decreasing $\langle y \rangle$ from 0.065 to 0.047. The ratio $R(x)$ obtained from this pion distribution is shown in Fig. 7(b). In this case, the slope of the data is reproduced very well. Again, use of the simple pion structure functions of Eqs. (2.28) and (2.29) causes significant changes only for $x < 0.05$.

V. CONCLUSIONS AND DISCUSSION

We began this investigation in order to establish whether the observed behavior vs x of the nuclear structure functions can be explained simply in a conventional nuclear model in which the deep-inelastic scattering occurs either from constituents of the nucleons or from constituents of the mesons associated with nuclear binding. We constrained ourselves to the use of structure functions measured on isolated nucleons and pions and attempted to fit the nuclear data in terms of convolutions over these free-nucleon and -meson structure functions. We conclude this approach is unable to fit the relatively large experimental effect represented by the central values of the data from the CERN EMC and the SLAC-MIT-Rochester experiments. We can achieve a quantitative fit to the data at *small* x only if we postulate an enhanced pion density $\langle n_\pi \rangle$ of about 0.4 extra pions per nucleon and/or make assumptions about the small-x behavior of the meson structure function which are inconsistent with available data. A density of 0.4 extra pions per nucleon in iron is roughly three times that provided by conventional nuclear models and is excessive. Such large values of $\langle n_\pi \rangle$ also result in inevitable serious discrepancies with the data on the ratio $R(x)$ at intermediate values of x $(0.3 < x < 0.5)$. These conclusions are insensitive to the methods we explored to enforce momentum balance between the meson and nucleon constituents of the nucleus. If we redefine our goal to be that of reproducing only the slope of $R(x)$ in the interesting region $0.05 < x < 0.5$, we find that we can achieve good results with acceptable structure functions and with values of $\langle n_\pi \rangle$ compatible with nuclear models.

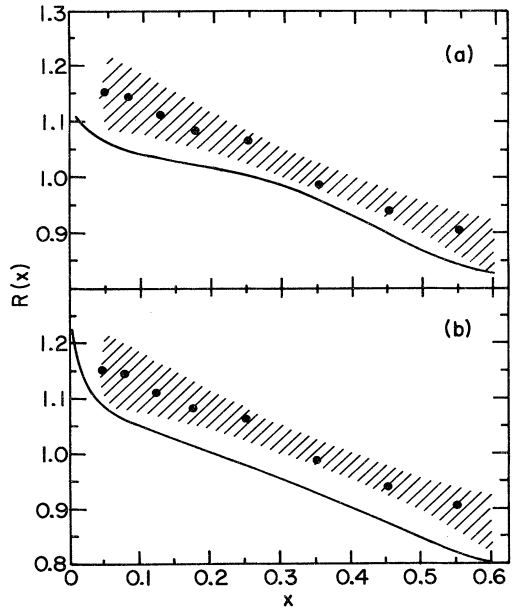

FIG. 7. Comparison of data and our model for $R(x)$, for Fe. (a) The solid curve of Fig. 6 is used for $f_\pi(y)$; $\langle n_\pi \rangle = 0.126$ and $\langle y \rangle = 0.065$. (b) The dotted curve of Fig. 6 is used for $f_\pi(y)$; $\langle n_\pi \rangle = 0.252$ and $\langle y \rangle = 0.047$.

In the data presented on $R(x)$, Q^2 and x are correlated such that the mean Q^2 grows substantially over the explored interval in x. In our study, we use input meson and nucleon structure functions whose full x dependence is specified at one fixed Q^2, which we take as $Q^2 \simeq 25$ GeV^2. We doubt whether our neglect to build the x, Q^2 correlation into our analysis affects our results in a substantial way, but the question warrants future study.

In Sec. III we present a formal analysis which demonstrates that the structure function of a compound system, such as a nucleus, whose constituents contribute incoherently, can be expressed as a linear functional of the structure functions of the constituents. We establish that this can always be done consistent with the requirements of Lorentz invariance and quantum mechanics. The resulting Eq. (1.1) is the basis for the remainder of the work in this paper.

Our failure to reproduce the data forces us to question the validity of our basic assumptions that structure functions of hadrons are unaffected by the nuclear medium and that hadrons contribute incoherently to the structure functions. We conclude that scattering from a proton in a nucleus is not described properly even at small and intermediate values of x by the free proton structure function. For whatever reasons, the nuclear medium enhances the effective nucleon structure function at small values of x. In order to fit the data, this "intrinsic" enhancement must be comparable to the enhancement of $F_2^A(x)$ at small x associated with scattering from the mesons in the nucleus associated with nuclear binding.

ACKNOWLEDGMENT

This work was performed under the auspices of the United States Department of Energy.

*High Energy Physics Division, Argonne National Laboratory, Argonne, IL 60439.

†Physics Division, Argonne National Laboratory, Argonne, IL 60439.

[1]European Muon Collaboration, J. J. Aubert *et al.,* Phys. Lett. 123B, 275 (1983); Rochester-SLAC-MIT Collaboration, A. Bodek *et al.,* Phys. Rev. Lett. 50, 1431 (1983); 51, 534 (1983).

[2]R. L. Jaffe, Phys. Rev. Lett. 50, 228 (1983).

[3]See, however, N. N. Nikolaev, Sov. Phys. Usp. 24, 531 (1981).

[4]See, e.g., W. Furmanski and A. Krzywicki, Orsay Report No. LPTHE Orsay 83/11, 1983 (unpublished); J. Szwed, Phys. Lett. 128B, 245 (1983). Other references to modified nuclear structure functions include G. Berlad, A. Dar, and G. Eilam, Phys. Rev. D 22, 1547 (1980); G. Baym, Physica 96A, 131 (1979); A. Krzywicki, Phys. Rev. D 14, 152 (1976); H. J. Pirner and J. P. Vary, Phys. Rev. Lett. 46, 1376 (1981); L. L. Frankfurt and M. I. Strickman, Phys. Rep. 76, 215 (1981); Nucl. Phys. B181, 22 (1981); M. Chemtob, Nucl. Phys. A336, 299 (1980); C. E. Carlson and T. J. Havens, Phys. Rev. Lett. 51, 261 (1983).

[5]C. H. Llewellyn Smith, Phys. Rev. Lett. 128B, 107 (1983); M. Ericson and A. W. Thomas, *ibid.* 128B, 112 (1983).

[6]G. Grammer and J. D. Sullivan, in *Electromagnetic Interactions of Hadrons,* edited by A. Donnachie and G. Shaw (Plenum, New York, 1978), Vol. 2, p. 195.

[7]Important shadowing effects ($R < 1$) may be expected at very small x; see, e.g., A. Mueller, in *Quarks, Leptons, and Supersymmetry,* Vol. 1 of *Proceedings of the XVIIth Rencontre de Moriond, Les Arcs, France, 1982,* edited by J. Trân Thanh Vân (Editions Frontières, Gif-Sur-Yvette, 1982), and references therein.

[8]CERN-Dortmund-Heidelberg-Saclay collaboration, F. Eisele, in *Proceedings of the 21st International Conference on High Energy Physics, Paris, 1982,* edited by P. Petiau and M. Porneuf [J. Phys. (Paris) Colloq. 43, C3-337 (1982)], and private communications.

[9]Since the strange-quark and strange-antiquark densities enter Eq. (2.14) with the small weight $e_s^2=\frac{1}{9}$, we note that the assumption of SU(3) symmetry for the ocean does not affect our results in any major way. For example, if we write $s(x)=\bar{s}(x)=0.5\,S(x)$, the coefficient $\frac{4}{3}$ in Eqs. (2.17) and (2.21) changes to $\frac{4}{3}-\frac{1}{9}=\frac{11}{9}$.

[10]Saclay–CERN–College de France–Ecole Polytechnique–Orsay Collaboration (CERN NA3 experiment), J. Badier *et al.,* Z. Phys. C 18, 281 (1983). See, also, C. B. Newman *et al.,* Phys. Rev. Lett. 42, 951 (1979); K. J. Anderson *et al., ibid.* 43, 1219 (1979); J. Varela *et al.,* CERN NA10 collaboration, Ecole Polytechnique Report No. LPNHE/X 83-02 (unpublished). For a recent review, see E. L. Berger, in *Particles and Fields—1982,* proceedings of the Meeting of the Division of Particles and Fields of the APS, College Park, Maryland, edited by W. E. Caswell and G. A. Snow (AIP, New York, 1982), p. 312.

[11]If a complete description of Q^2 dependence is desired, it may be more appropriate to begin with the expression $V_\pi(x)\propto(1-x)^2+c/Q^2$. See E. L. Berger and S. J. Brodsky, Phys. Rev. Lett. 42, 940 (1979). For the purposes of the present paper, however, the effective pion structure function obtained from the NA3 analysis should suffice.

[12]R. Blankenbecler and S. J. Brodsky, Phys. Rev. D 10, 2973 (1974); S. J. Brodsky and G. Farrar, *ibid.* 11, 1309 (1975).

[13]In the terminology of P. A. M. Dirac, Rev. Mod. Phys. 21, 392 (1949), the relativistic dynamics used in the following is "front form" dynamics. For a discussion of relativistic quantum mechanics of interacting particles, see F. Coester and W. N. Polyzou, Phys. Rev. D 26, 1348 (1982), and references therein.

[14]A. Bodek and J. L. Ritchie, Phys. Rev. D 23, 1070 (1981); 24, 1400 (1981).

[15]B. D. Day (private communication). We thank Dr. Day for supplying us the nucleon momentum distribution obtained from his nuclear-matter calculations using the Paris potential; B. D. Day, Phys. Rev. C 24, 1203 (1981).

[16]B. L. Friman, V. R. Pandharipande, and R. B. Wiringa, Phys. Rev. Lett. 51, 763 (1983); see Eq. (6).

[17]F. Coester, in *Quanta,* edited by P. G. O. Freund, C. J. Goebel, and Y. Nambu, (University of Chicago Press, Chicago, 1970), p. 147; see Eq. (74).

[18]R. B. Wiringa, R. A. Smith, and T. L. Ainsworth (unpublished).

[19]At. Data. Nucl. Data Tables 14, 479 (1974).